ISBN 978-93-5156-328-0
International Conference of Advance Research and Innovation (ICARI-2015)

Simulation of Injector in Cold Spray Process by Fluent-6

Sameer Kumar, Md. Zunaid *, Qasim Murtaza, N.A. Ansari, Akhilesh Arora
Department of Mechanical Engineering, Delhi Technological University, New Delhi, India

Article Info
Article history:
Received 9 January 2015
Received in revised form
15 January 2015
Accepted 22 January 2015
Available online 31 January 2015

Keywords
Cold-spray process;
Critical Velocity;
Injector;
Coating

Abstract

The cold spray process is a modern coating process using high velocity and low process temperature particles for surface modification to improve the surface properties of the substrate, such as adhesion, wettability, corrosion resistance, or wear resistance. Coating may be applied as liquid, gases, or solid. In this process spray particles are accelerated the high velocity by a supersonic gas flow that is generated through only by convergent-divergent (CD) nozzle. Convergent-divergent nozzle could achieve the super-sonic velocity through the divergent section, but there is also some problem if the velocity is greater than the Mach number at the throat then the nozzle would be chocked and no flow of air and particles through the nozzle. In this study, simulation and optimization of the cold spray nozzle and spray process has been done with the help of Modelling software. Cold spray nozzle geometry of (CD) nozzle drawn in GAMBIT and solved by the FLUENT solver. To solve the cold spray nozzle, pressure based solver is used because it is more relevant for the problem, for turbulence model Realizable k-ε flow model has used in this problem because this model is relatively new and differ from the standard k-ε model by two ways firstly it contain a new formulation for turbulence viscosity and secondly it has new transport equation for the dissipation rate. After that providing the operating and boundary condition at the inlet and outlet section of the (CD) nozzle, the discrete phase model is activated. Optimizations of CD nozzle is done at the group injection for the length 10mm, 20mm and 30mm after giving the all parameters and then validate the respective work.

1. Introduction

Coating is a covering that is applied to the surface of an object, usually referred as the substrate. The purpose of applying the coating may be decorative, functional, or both. The coating itself may be an all-over coating, completely covering the substrate, or it may only cover parts of the substrate. Functional coating may be applied to change the surface properties of the substrate, such as adhesion, wettability, corrosion resistance, or wear resistance. Coating may be applied as liquid, gases, or solid. Now a day's Coating technology is growing because of its important role in improving, e.g., corrosion resistance, conductivity, and other properties of material in order to decrease costs and increase service life and safety. Thermal spray processes, including flame, arc, plasma, high velocity oxygen fuel (HVOF) and cold spraying, are the techniques to produce coatings from powder or wire feedstock by spraying molten, semi-molten or solid particles on the substrate and forming the coating. Acceleration of particles can be done by several ways based on energy used: electrical (arc and plasma spraying), chemical (flame and HVOF spraying), or kinetic (cold spraying) energy.

Cold spraying is a coating process which enables production of metallic and metallic ceramic coating with dense (very low porosity level) and pure (low oxygen content) structures. Several coating applications such as corrosion resistance and electrical conductivity rely on these properties. Generally, cold spraying is based on higher particle velocities and lower process temperature than other thermal spray process.

Corresponding Author,
E-mail address: mzunaid3k@gmail.com

Cold gas spraying is a relatively new coating process by which coatings can be produced without significant heating of the sprayed powder. There is a contrast b/w Thermal spray and in Cold spray. In the well-known thermal spray processes such as flame, arc, and plasma spraying is used, on the other hand in cold spraying there is no melting of particles prior to impact on the substrate. The adhesion of particles in this process is due solely to their kinetic energy upon impact. Experimental investigations show that successful bonding is achieved only above a critical particle velocity, whose value depends on the temperature and the thermo mechanical properties of the sprayed material [1].

Cold-Gas Dynamic Spray or simply Cold Spray is a process of applying coatings by exposing a metallic or dielectric substrate to a high velocity (300 to 1200 m/s) jet of small (1 to 50 μm) particles accelerated by a supersonic jet of compressed gas. This process is based on the selection of the combination of particle temperature, velocity, and size that allows spraying at the lowest temperature possible. In the Cold Spray process, powder particles are accelerated by the supersonic gas jet at a temperature that is always lower than the melting point of the material, resulting in coating formation from particles in the solid state. As a consequence, the deleterious effects of high temperature oxidation, evaporation, melting, crystallization, residual stresses, gas release, and other common problems for traditional thermal spray methods are minimized or eliminated.

Cold spraying is an emerging coating process which is differed from the well-known thermal spray processes in which flame, arc, and plasma spraying is used, on the other hand the powders does not melt in Cold spray before

impacting the substrate. This character makes cold spray process commendable for many different coating applications dealing with various materials, not only with metals but also with polymers, composites, etc. Bonding of the particles in this process occurs due to the high kinetic energy upon impact; therefore, the velocity of the particle plays the most important role in material deposition. During the process, powders are accelerated by injection into a high velocity stream of gas.

The high velocity stream is generated through a converging–diverging nozzle. As the process continues, the particles impact the substrate and form bonds with it, resulting in a uniform almost porosity-free coating with high bonding strength [2]. Low temperature also aids in retaining the original powder chemistry and phases in the coating, with changes only due to deformation and cold-working. Bonding of particles in cold gas spraying is presumed to be the result of extensive plastic deformation and related phenomena at the interface [3]. It is to be underlined that the particles remain in the solid state and are relatively cold, so the bulk reaction on impact and the cohesion of the deposited material is accomplished in solid state. Schematic diagram of the cold spray equipment is shown in Fig. 1. Resource by Sameer Kumar M.tech. M.E.D. D.T.U. Delhi Thesis [20]

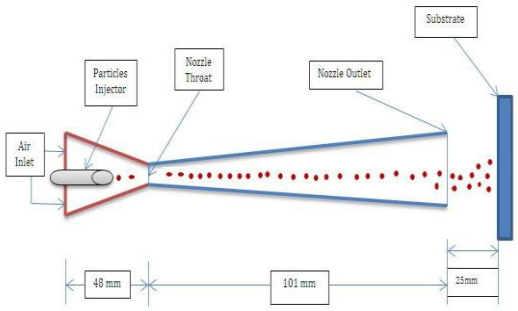

Fig: 1. Schematic Diagram of the Cold Spray

Show main parts of the nozzle with dimensions, D_{inlet} = 18 mm; D_{outlet} = 8.35 mm; D_{throat} = 2.7 mm; $L_{conv.}$ = 48 mm; $L_{div.}$ = 101 mm, Stand-off Distance = 25 mm, which are always fixed during the project work.

2. Simulation Procedure

The first step in the approach towards solution procedure is to divide the nozzle Length L, into a number of divisions (div), the numerical integration is carried out in each division to find the variation of the main parameters with length. The main parameters are those parameters that change during the course of the integration seven main parameters are used in this analysis. These parameters are

$T_{air,in}$– Temperature of inlet; $T_{air,outlet}$– Temperature of outlet; $V_{air,in}$- velocity of air at inlet,P_{in}- Pressure at inlet of Injector; D_p -Diameter of Particles; $V_{p,in}$- Inlet Velocity of particles; $V_{p,out}$- Outlet Velocity of particles.

The lagging parameters on the other hand are assumed to be constant during the individual elements of integration. These parameters include kinematic viscosity, density of air, heat transfer coefficient, Lewis factor etc. The lagging parameters are recalculated using the main parameters at every division. These parameters along with the main parameters serve as a fresh input to the solver for the subsequent interval or division. The above discussion holds good for single as well as multi-diameter droplets model. In multi-diameter droplets model, the different equations of main parameters for different droplets are numerically integrated separately.

1. Boundary Conditions

The input is boundary conditions which for parallel downward flow are:

a) Nozzle Geometry: Inlet, Throat, Outlet, cross section area and Injector of the nozzle.
b) Spray characteristics: Particles velocity, angle of projection, mean diameter of Particles model and diameter range (5-50) µm.
c) Inlet air conditions: Air or Nitrogen velocity, Pressure.
d) Particles Inlet Condition: Mass flow rate and its temperature at inlet and Pressure.

Table: 1. Input Data Parameters of Copper

Parameters	Cu	Ni	SS316
Density (kg./m^3)	8960	8900	8031
Conductivity (W/km2)	386	90.9	16
Specific Heat (J/KgK)	383	435-446	457
Melting Point (K)	1356	1727	1643
C.V. (m/s)	420	520	470
Poisson ratio	0.34	0.31	0.3
Module of elasticity (GPa)	124	200	193

Resource: R. Ghelichi [3].

Data collected through above table 1 consider the Copper as the Injector Powder for the project because in the FLUENT-6 Copper is more easy to use compare to other materials.

2. Make Nozzle geometry by GAMBIT

Step 1: Open the exceed software after that open GAMBIT 2.4.6.

Step 2: Open the operation geometry command after that opens tool pads that allow me to create and modify model geometry.

Step 3: After that in the geometry function (vortex command) opens a sub-pad, related to operations involves vertices.

Step 4: Now by co-ordinate system draw geometry of nozzle by point's co-ordinate.

Step 5: Now go to the edge command open a sub-pad related to operation involving edges first main geometry of nozzle.

Step 6: Now go face geometry select all edges for make face. Face forms a real or virtual face from existing topological entities.

Step 7: After that go to on the command of operation-mesh edge command, open a sub-pad related to operation involving edges. After that generate the mesh with give the spacing according to the need interval count.

Step 8: for finalized the nozzle must give the boundary condition like inlet, outlet, wall etc. After that save as

the file with some name and finally Export file as (.msh) format to read in FLUENT 6.

Table: 2. Input Parameters of Nozzle

Parameters	Cold Spray Machine
Nozzle Mach	1.5-2.6
Working Pressure	1.5, 2.5& 3.0 MPa
Gas Temperature	30-500 ℃
Working Gas (Ideal-Gas)	Air
Gas flow Rate	18-20 gm/sec
Particle Diameter (Uniform)	20 µm
Diameter of Throat	2.7 mm
Stand Off Distance	25mm
Inlet Diameter of Nozzle	18.2 & 18 mm
Throat Diameter	2.7 mm
Exit Diameter	8.35 mm
Convergent Length	54 & 48mm
Divergent Length	67.6 & 101 mm
Powder Injector Diameter	2 mm
Powder Injector Length	10,20,25 & 30 mm
Particle Powder	Copper
Intake Particles Velocity	20-30 m/sec
Mass Flow rate	10 gm/sec

Resource: Sung Hwan Jang et al., [7] & .T.Van steenkiste et al., [12].

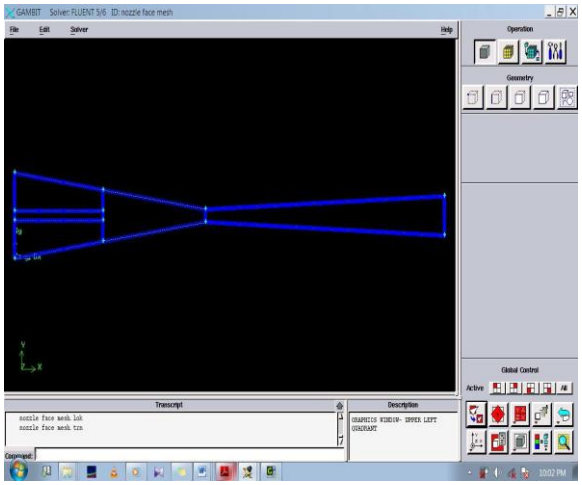

Fig: 2. Show First main nozzle Geometry

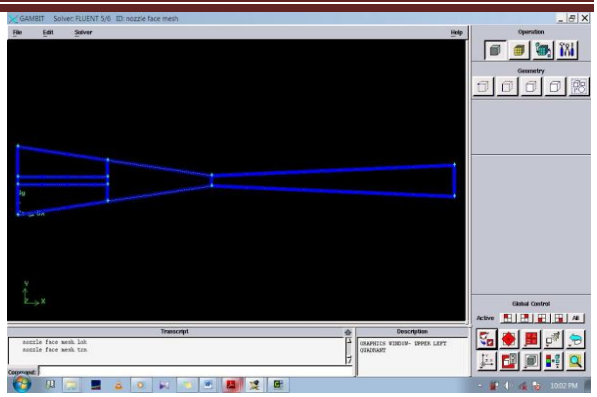

Fig: 3. Show Nozzle with Interval Count and Spacing

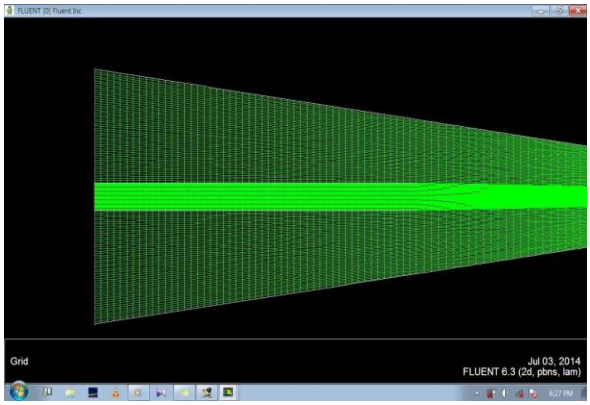

Fig: 4a.

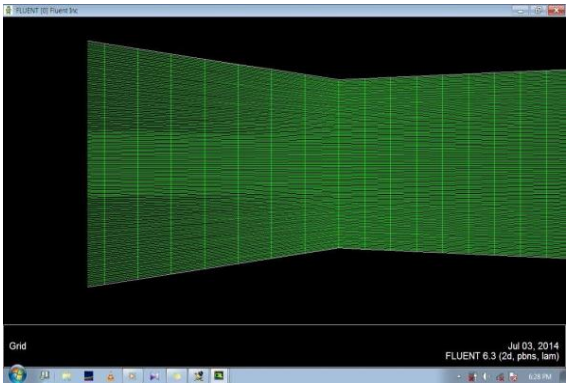

Fig: 4b

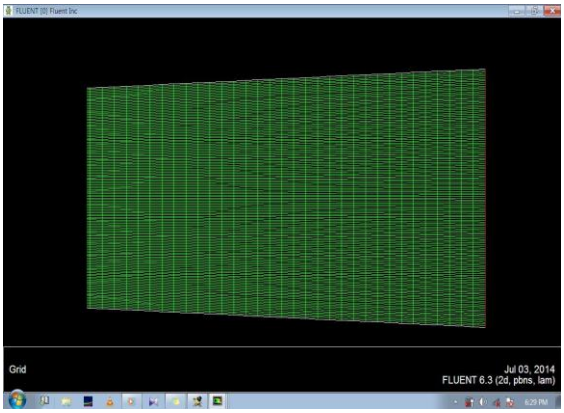

Fig: 4c

ISBN 978-93-5156-328-0

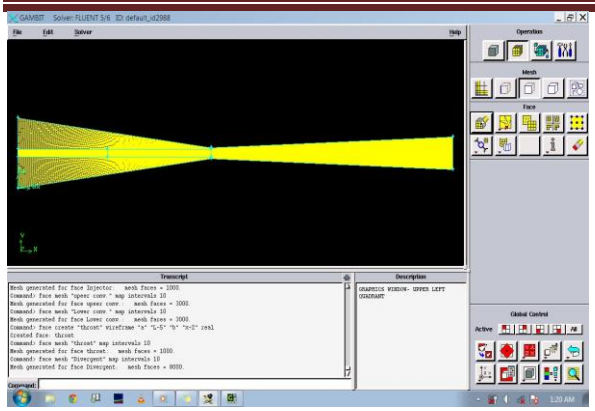

Fig: 5. Final Nozzle with Boundary Conditions

Figure 4 a. b. & c. Figure shows Mesh faces at the convergent, throat and Divergent section of the nozzle. Nozzle inlet, throat and divergent sections have 150 interval counts, lower & upper part of convergent and divergent nozzle have 100 & 150 interval counts respectively with 10 spacing by each sections. Resource by Sameer Kumar M.tech. Thesis M.E.D. D.T.U. Delhi [20]

3. Flow Chart of Simulation Process the Project Paper

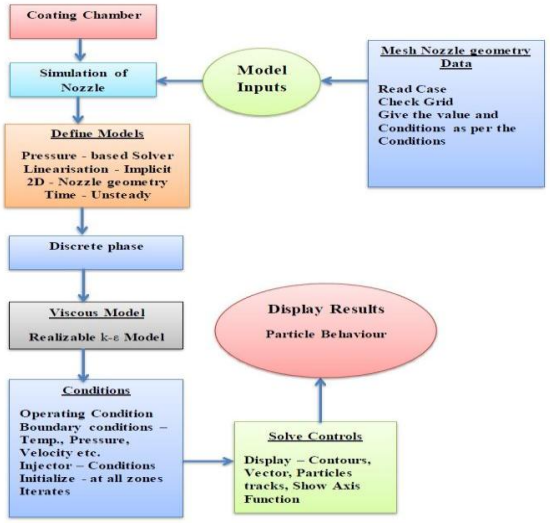

Fig: 6. Flow Chart of Cold spray Modelling with discrete Phase

3.1 Transport Equations for the Realizable k-ε Model

The modeled transport equations for k and ε in the realizable k- ε model are:

$$\frac{\partial}{\partial t}(\rho k)+\frac{\partial}{\partial x_j}(\rho k u_j)=\frac{\partial}{\partial x_j}\left[\left(\mu+\frac{\mu_t}{\sigma_k}\right)\frac{\partial k}{\partial x_j}\right]+G_k+G_b-\rho\epsilon-Y_M+S_K \quad (3.1)$$

and

$$\frac{\partial}{\partial t}(\rho \epsilon)+\frac{\partial}{\partial x_j}(\rho \epsilon u_j)=\frac{\partial}{\partial x_j}\left[\left(\mu+\frac{\mu_t}{\sigma_\epsilon}\right)\frac{\partial \epsilon}{\partial x_j}\right]+\rho C_1 S_\epsilon+\rho C_2\frac{\epsilon^2}{k+\sqrt{v\epsilon}}+C_{2\epsilon}\frac{\epsilon}{k}C_{3\epsilon}G_b+S_\epsilon \quad (3.2)$$

Where

$$C_1=max\left[0.43,\frac{\eta}{\eta+5}\right];$$

$$\eta=S\frac{k}{\varepsilon}\ ;\ S=\sqrt{2S_{ij}S_{ij}}$$

In these equations,

G_k- represents the generation of turbulence kinetic energy due to the mean velocity gradients, calculated as Modeling Turbulent Production in the k- ϵ Models.

G_b- is the generation of turbulence kinetic energy due to buoyancy, calculated as Effects of Buoyancy on Turbulence in the k- ϵ Models.

Y_M - represents the contribution of the fluctuating dilatation in compressible turbulence to the overall dissipation rate, calculated as Effects of Compressibility on Turbulence in the k- ϵ Models.

$C_{1\epsilon}$, $C_{2\epsilon}$ and $C_{3\epsilon}$ are constants. α_k And α_ϵ are the inverse effective Prandtl numbers for k andϵ, respectively. S_K And S_ϵ are user-defined source terms

Note that the k equation is the same as that in the standard k- ϵ model and the RNG k- ϵ model, except for the model constants [14].

Applying the fundamental laws of mechanics to a fluid gives the governing equations for a fluid. The conservation of mass equation is

$$\frac{\partial \rho}{\partial t}+\nabla.\left(\rho\vec{V}\right)=0 \quad (3.3)$$

And the conservation of momentum equation is

$$\rho\frac{\partial \vec{v}}{\partial t}+\rho\left(\vec{V}.\nabla\right)\vec{V}=-\nabla p+\rho\vec{g}+\nabla.\tau_{ij} \quad (3.4)$$

These equations along with the conservation of energy equation form a set of coupled, nonlinear partial differential equations. It is not possible to solve these equations analytically for most engineering problems [16].

4. Isentropic Gas Flow Model

The following equation relates the gas temperature at the throat (*T**) to the total gas temperature (note all quantities given with an * is throat or sonic conditions):

$$\frac{T_0}{T^*}=1+\frac{\gamma-1}{2} \quad (4.3.1)$$

Where γ is the ratio of specific heats. For monatomic gases, γ is 1.66, and for diatomic gases γ is typically 1.4 (Air is typically modeled as a diatomic gas because it is a mixture of nitrogen and oxygen.) Larger molecules have even lower specific heat ratios, but are typically not used in thermal spray applications. Equation (4.3.1) assumes that the throat condition is sonic. Sonic conditions are only

obtained for sufficient stagnation gas pressures, but this condition is usually obtained for all thermal spray applications. At the throat, the Mach number is unity, and the local velocity can be obtained from;

$$V^* = \sqrt{\gamma R T^*} \quad (4.3.2)$$

Where *R* is the specific gas constant (the universal gas constant divided by the gas molecular weight) . Equation 2 illustrates why it is often found that helium makes a better carrier gas due to its smaller molecular weight and higher specific heat ratio.

A mass balance yields the throat density:

$$\rho^* = \frac{\dot{m}}{V^* A^*} \quad (4.3.3)$$

At this point, the throat area (*A**) can be set to unity and the mass flow rate $(\dot{m})$ specified as a flux per unit throat area. This allows obtaining a single solution that can then be easily scaled by the throat area if desired.

Using the perfect gas law, the throat pressure $P^*$is obtained:

$$P^* = \rho^* R T^* \quad (4.3.4)$$

From the throat pressure, the stagnation pressure P_0 can be calculated:

$$\frac{P_0}{P^*} = \left(1 + \frac{\gamma-1}{2}\right)^{\frac{\gamma}{\gamma-1}} \quad (4.3.5)$$

If sonic conditions are to be maintained at the throat, the throat pressure must be above the ambient, or spray chamber, pressure. To complete the gas dynamic calculation, a single nozzle exit condition needs to be specified. This could be the exit pressure, exit velocity, exit Mach number, or exit area. The gas exit pressure need not match the ambient pressure. Current cold-spray gun operating conditions have an exit pressure well below ambient to obtain maximum spray particle velocities. Thus, the gas flow is said to be over expanded. This results in a flow outside of the nozzle that cannot be solved by simple one-dimensional gas dynamic equations. However, the one-dimensional results presented here still apply inside the nozzle as long as the overexpansion is not so great as to cause a normal shock inside the gun. Shocks inside the gun have not been predicted in operational conditions tested at Sandia to this point [5].

It is assumed here that the exit area is specified. The following equation is used to obtain the exit Mach number when the exit area is specified:

$$\frac{A}{A^*} = \left(\frac{1}{M}\right)\left[\left(\frac{2}{\gamma+1}\right)\left(1 + \frac{\gamma-1}{2} M^2\right)\right]^{\frac{\gamma+1}{2(\gamma-1)}} \quad (4.3.6)$$

With the exit Mach number known, the other gas conditions can be obtained from the following isentropic relationships:

$$\frac{P}{P^*} = \left[\left(\frac{\gamma+1}{2+(\gamma-1)M^2}\right)\right]^{\frac{\gamma}{(\gamma-1)}} \quad (4.3.7)$$

$$\frac{T_0}{T} = 1 + \frac{\gamma-1}{2} M^2 \quad (4.3.8)$$

$$V = \sqrt{\gamma R T} \quad (4.3.9)$$

$$\frac{\rho_0}{\rho} = \left(1 + \frac{\gamma-1}{2} M^2\right)^{\frac{\gamma}{(\gamma-1)}} \quad (4.3.10)$$

Because the exit pressure calculated is typically less than ambient, a simple check is required to make sure the given solution is possible. The following calculation yields a trial pressure for the design. *P*s is the downstream shock pressure that would be obtained if a shock occurred at the nozzle exit:

$$\frac{P_s}{P_c} = \left(\frac{2\gamma}{\gamma+1} M_c^2 - \frac{\gamma-1}{\gamma+1}\right) \quad (4.3.11)$$

Equations (4.3.1) through (4.3.4) and (4.3.6) through (4.3.10) can also be used to simulate plasma or HVOF spray systems by assuming an isentropic expansion from the throat to the exit of a diverging nozzle.

However, the total gas temperature must be obtained through an energy balance. The total gas temperature is greater than the incoming gas temperature due to the energy additions. So, in place of (Eq. 4.3.5) (to calculate the stagnation pressure), another relation must be substituted. Reasonable agreement with experimental data has been obtained using a Rayleigh Line calculation instead of the isentropic assumption. The Rayleigh Line calculation assumes a constant area energy addition [5].

4.1 Check Back Flow at Injector, Inlet and Outlet

Fig: 7a.

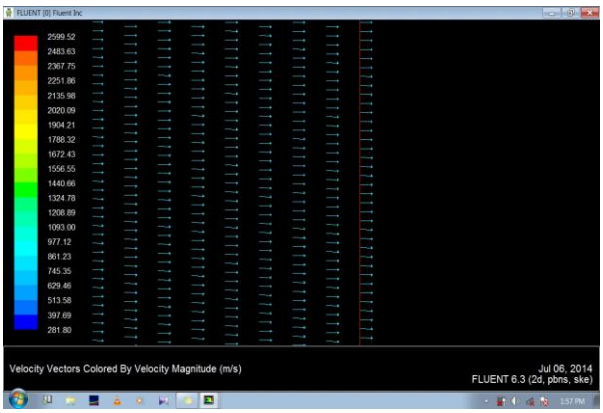

Fig: 7b.

Fig: 7a & 7b shows there is not any back flow at the Convergent and Injector Of the nozzle & Divergent Section of the nozzle respectively

4.2 Validation by H. Fukanuma et al. [1]

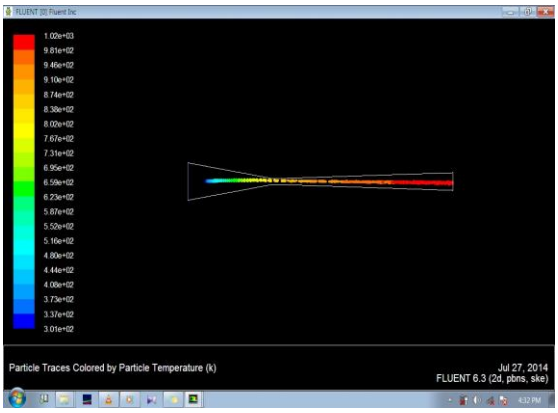

Fig: 8a

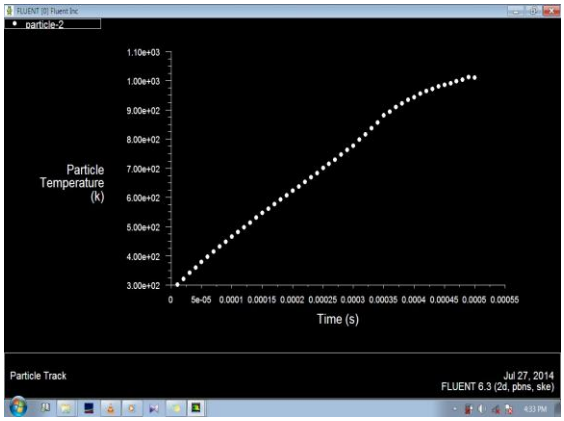

Fig: 8b

Fig: 8a. Shows that maximum Temp of Particles at outlet of the nozzle is 1002 K & Figure 8b- Graph shows that maximum Temp of Particles at outlet of the nozzle is 1002 K and the temp. is continuously increase with respect to Time as well as Length of Nozzle.

Figure 8c & 8d - Maximum Velocity of Particles at outlet of the nozzle is 680 m/sec, Velocity of particles firstly increase slowly and smoothly but after the throat it increase very rapidly and achieved 680 m/sec speed at the exit of nozzle.

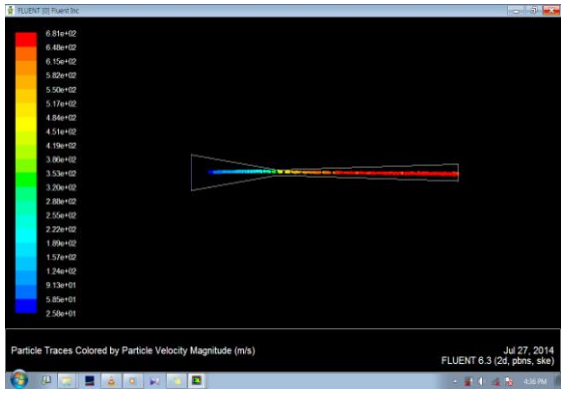

Fig: 8c

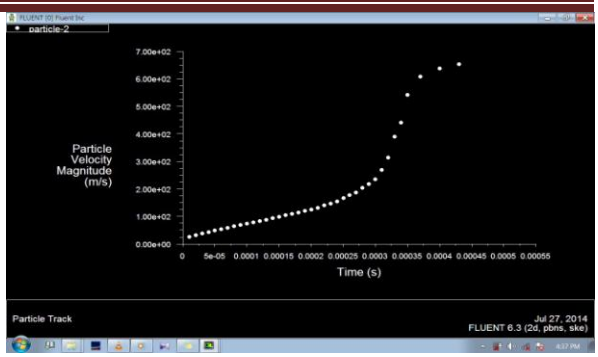

Fig: 8d.

5. Result and Discussion

The data which have been taken in this paper to solve the project problem. By this data we have to find many other results with fixed dimensions of the nozzle instead of injector length. By the data of table this is clear that in this simulation we have to use three different types of injector which have same diameter 2 mm. In this simulation we have taken total four type of different velocity of Air at the inlet section of the nozzle; these are 350, 370, 390 and 410 m/sec. for the 10, 20 and 30 mm length of injector simultaneously. Input parameters are given by according to the table no. 3

Table: 3.

S.NO	V_{air} Inlet	V_p Inlet (m/sec)	T_{air} inlet (K)	V_p outlet (m/sec)	T_p Outlet (K)	Injection Length (mm)
1	350	30	400	560	348	10
2	350	30	400	566	343	20
3	350	30	400	544	337	30
4	370	30	400	545	350	10
5	370	30	400	575	344	20
6	370	30	400	571	335	30
7	390	30	400	627	448	10
8	390	30	400	652	342	20
9	390	30	400	622	334	30
10	410	30	400	691	347	10
11	410	30	400	655	342	20
12	410	30	400	652	334	30

After giving all input parameters for the injector length 10, 20, 30mm following result would be found and collected in the form of several cases.

CASE 1 (S.No. 1-3)

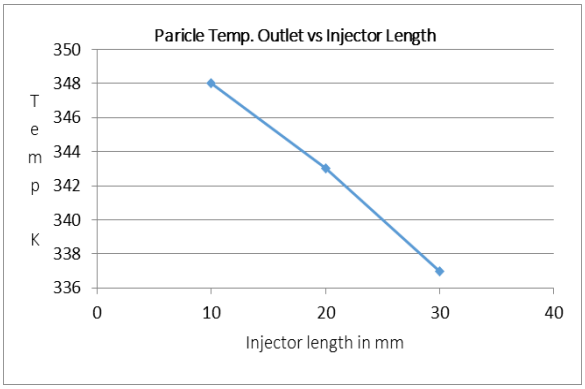

Fig: 9.

ISBN 978-93-5156-328-0

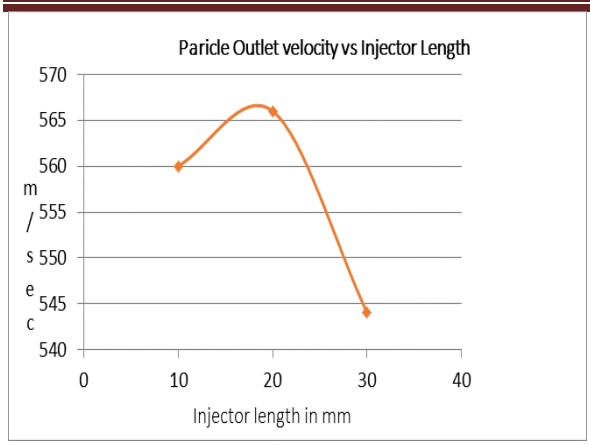

Fig: 10.

In this case 1 V_{air} inlet was taken 350 m/sec and length of injector are 10 mm, 20mm and 30mm respectively increase in the nozzle. The temperature was affected due to the variation of injector length and it was seen that as increase the injector length the temperature will be decrease at the outlet of the nozzle.

In other hand the velocity of particles Firstly increase near by the 20 mm length of injector after that it will be decreases simultaneously.

CASE 2 (S.No. 4-6)

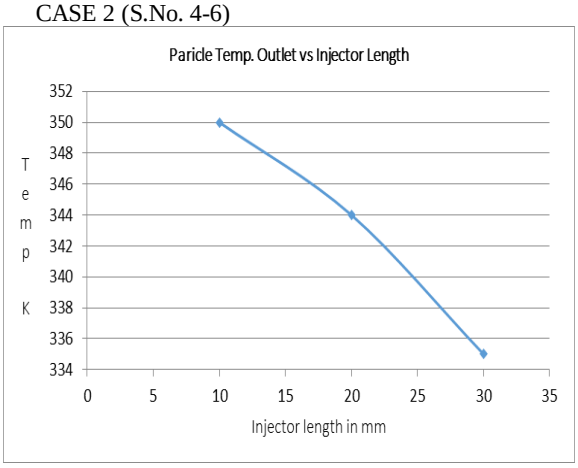

Fig: 11.

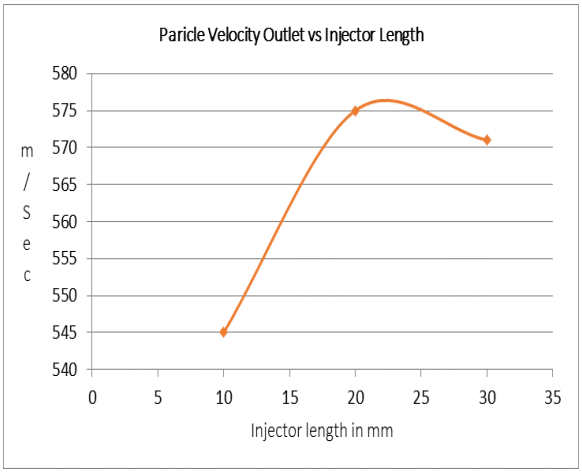

Fig: 12.

In this case 2 V_{air} inlet was taken 370 m/sec and length of injector are 10 mm, 20mm and 30mm respectively increase in the nozzle. The temperature was affected due to the variation of injector length and it was seen that as we have increase the injector length the temperature will be decrease at the outlet of the nozzle.

In other hand the velocity of particles firstly increases near by the 20 mm length of injector after that it will be decreases simultaneously.

CASE 3 (S. No. 7-9)

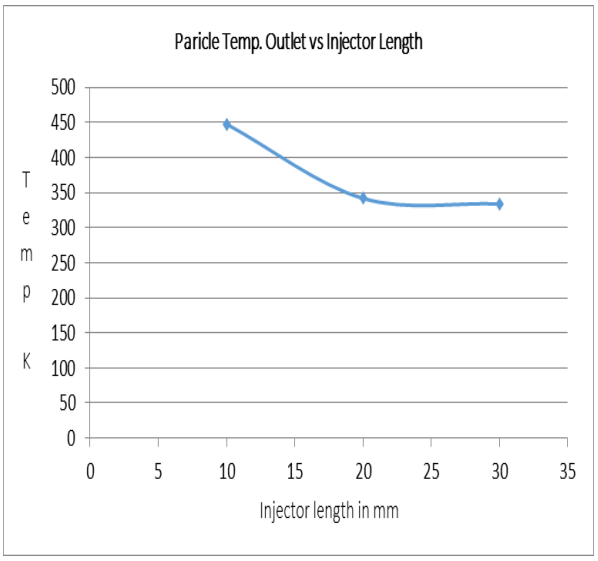

Fig: 13.

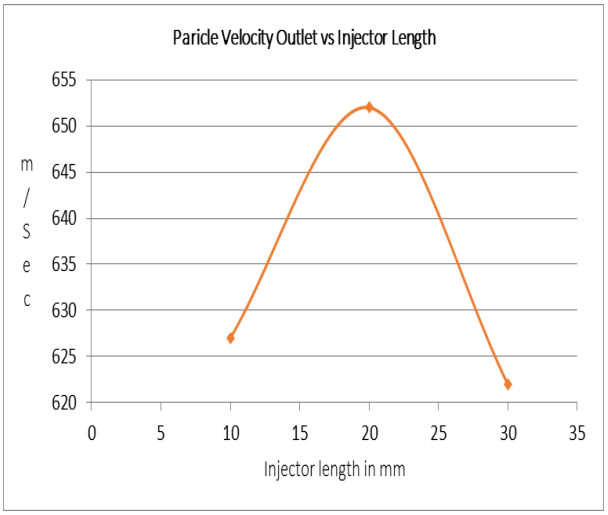

Fig: 14.

In this case 3 Vair inlet was taken 390 m/sec and length of injector are 10 mm, 20mm and 30mm respectively increase in the nozzle. The temperature was affected due to the variation of injector length and it was seen that as we have increase the injector length the temperature will be decrease up to 20 mm length and after that there is no decrement in the temperature.

In other hand the velocity of particles Firstly increase up to the 20 mm length of injector after that it will be decreases simultaneously.

CASE 4 (S. No. 10-12)

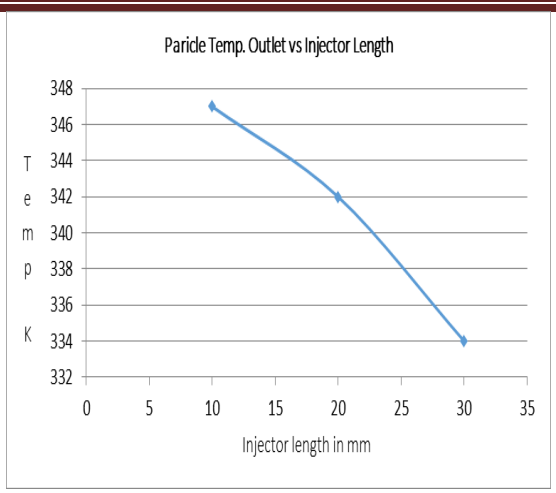

Fig: 15.

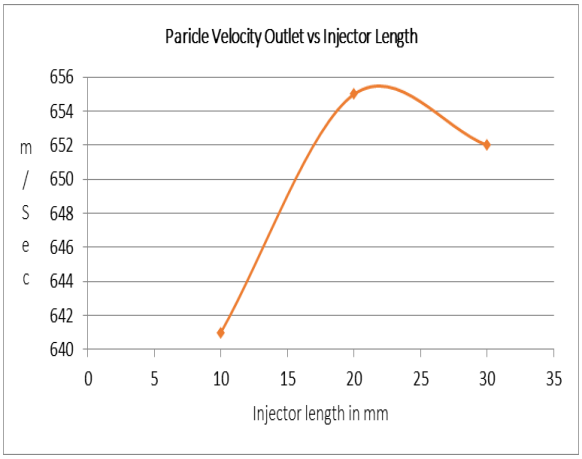

Fig: 16.

In this case 4 Vair inlet was taken 410 m/sec and length of injector are 10 mm, 20mm and 30mm respectively increase in the nozzle. The temperature was affected due to the variation of injector length and it was seen that as we have increase the injector length the temperature will be decrease continuously.

In other hand the velocity of particles firstly increase near by the 20 mm length of injector after that it will be decreases simultaneously. That data from case 1 to case 4 have taken from the table 3.

6. Conclusions

1. This is very clear in the all cases (e.g. Case-1, case-2, case-3 and case-4) that the temperature of the particle is highest for the injector length 10mm and lowest for the injector length 30mm.
2. The result also shows that the temperature slightly decreases with increase the length of the injector.
3. While the temperature would be decrease linearly but this thing is not happened with the velocity of particles at the outlet of the nozzle. As well as the length of injector the velocity of particles firstly increase up to the 20mm length after that it would be decrease.
4. This is also found that the optimum result would be getting near by the 20 mm length of injection.

References

[1] H. Fukanuma, R. Huang Simulation of Cold Spray Nozzle Accompanying a Water cooling Adjustment, Plasma Giken Co., Saitama, Japan.

[2] A. Papyinyrin, The Development of the Cold Spray Process, Cold Spray Technology (CST), USA, 2006

[3] R. Ghelichi, Numerical simulation of cold spray coating, Surface & Coatings Technology, 205, 2011 5294–5301

[4] H. Assadi, F. Gartner, Bonding mechanism in cold gas spraying, Department of Materials Engineering, Tarbiat Modarres University, 2002

[5] R. C. Dykhuizen, M.F. Smith, Gas Dynamic Principles of Cold Spray, JTTEE5 7:205-212 ASM International, 1998

[6] X. Guo, Y. Niu, L. Huang, H. Ji, X. Zheng, Microstructure and Tribological Property of TiC-Mo Composite Coating Prepared by Vacuum Plasma Spraying, ASM International, 2012

[7] Sung-Hwan Jang, Sung-Han Park, Jeong-Whan Han, Chang-Hee Lee, Hyung-Jun Kim, Factors of Nozzle Design Affecting on Supersonic Flow in Cold Spray Process School of Materials Science and Engineering, Inha University, inchon, 402-751, South Korea, Trans Tech Publications, Switzerland, 2006

[8] S. V. Klinkov, V. F. Kosarev, A. A. Sova, I. Smurov, Deposition of multicomponent coatings by Cold Spray, Khristianovich Institute of Theoretical and Applied Mechanics SB RAS (ITAM SB RAS), 630090, Novosibirsk, Russia, 2008

[9] Wen-Ya Li, Hanlin Liao, Hong-Tao Wang, Chang-Jiu Li, Ga Zhang, C. Coddet, Optimal design of a convergent-barrel cold spray nozzle by numerical method State Key Laboratory for Mechanical Behavior of Materials, School of Materials Science and Engineering, 2005

[10] Wen-Ya Li, Hanlin Liao, G. Douchy, C. Coddet, Optimal design of a cold spray nozzle by numerical analysis of particle velocity and experimental validation with 316L stainless steel powder, LERMPS-UTBM, Site de Se´venans, 90010 Belfort Cedex, France

[11] Surface Engineering, CSIR- National Aerospace laboratories, Bangalore, 2006

[12] T. Van steenkiste, J. R. Smith, Evaluation of coating Produced via kinetic and Cold Spray Processes, 2003

[13] V. Champagne, The Cold Spray Materials Deposition Process, Fundamentals and Application, Wood head publishing, 2007

[14] FLUENT 6.3 User's Guide, Chapter Modeling Turbulence

[15] A. Amsden, P. J. O'Rourke, T. D. Butler. KIVA-2:, A Computer Program for Chemically Reactive Flows with Sprays. Technical Report LA-11560-MS, UC- 96, Los Alamos National Laboratory, Los Alamos, New Mexico

[16] Q. Murtaza, J. Stokes, M. Ardhaoui, Computational fluid dynamics analysis of the production of bio-thermal spray hydroxyapatite powders, Int. J. Computational Materials Science and Surface Engineering, 5(1), Materials Processing Research Centre (MPRC), Dublin City University, 2012

[17] Rajesh Bhaskaran, Lance Collins, Introduction to CFD Basics.
[18] J. M. McDonough, LECTURES in COMPUTATIONAL FLUID DYNAMICS of INCOMPRESSIBLE FLOW: Mathematics, Algorithms and Implementation, Departments of Mechanical Engineering and Mathematics, University of Kentucky, 2007
[19] Lecture 4, Computational engineering Introduction to numerical methods, FVM, 2006
[20] S. Kumar, M.E.D. Delhi College of engineering thesis, 2012-14